On the finite element formulation of dynamic two-phase coupled problems

Annamaria Cividini *, Giancarlo Gioda [1]

Department of Architecture, Built Environment and Construction Engineering, Politecnico di Milano, Piazza Leonardo da Vinci 32, 20133 Milano, Italy

Two finite element approaches are discussed for the analysis of the coupled problems of seepage and deformation of saturated porous media in the presence of an acceleration field varying in time and space (e.g. during an earthquake). The equations governing the two phase problem in dynamic regime are recalled first under assumptions which seem reasonable in the geotechnical context. Then they are cast into a first finite element form without introducing further assumptions with respect to those adopted in deriving them. Subsequently, a simplified formulation is presented which requires a reduced number of nodal variables with respect to the first one. After discussing a time integration scheme, the two approaches are applied to the solution of a benchmark example and some comparative comments are presented on their accuracy and on the required computational effort.

Keywords:
Finite element
Dynamic analysis
Saturated granular soil
Shallow excavation

1. Introduction

The problem discussed here is related to the design of deep retaining structures, such as diaphragm walls, in seismic regions. In particular, the case of excavations in granular soils below the water table is considered.

In these conditions the assessment of the effects of earthquakes on the stability and deformation of the structure requires the evaluation of the dynamic effective stresses and pore pressure that the saturated soil exerts on it. Note, in fact, that the relatively high hydraulic conductivity of granular soils rules out the assumption of undrained conditions sometime adopted in engineering practice when dealing with cohesive materials.

In relatively simple cases, e.g. gravity retaining walls, this problem can be tackled through well-established theories such as those originally proposed by Okabe in 1926 [1] and by Mononobe and Matsuo in 1929 [2] for the evaluation of the effective pressure, and by Westergaard in 1933 [3] for estimating the dynamic increase of water pressure. In more complex conditions, however, a coupled dynamic analysis of seepage flow and deformation of the soil skeleton is required.

In quasi static conditions, i.e. under a gravity acceleration field constant in time and space, broadly accepted numerical approaches are available for the numerical analysis of seepage and of the coupled effective stress-flow problem, e.g. [4–6].

When the acceleration field varies with time, e.g. during earthquakes, the analysis of seepage becomes less straightforward since recourse cannot be made anymore to the usual concept of hydraulic head [7,8]. This led, in turn, to various numerical approaches for dynamic coupled problems that involve different assumptions and different sets of independent variables [9–12].

The complex mathematical structure of the dynamic two-phase problem does not permit a straightforward evaluation of the consequences of these assumptions and, hence, makes the choice of the most appropriate numerical approach somewhat controversial.

Here, a previous study concerning the numerical analysis of dynamic seepage [13–15] is extended to the coupled two-phase analysis. This work neglects the possible development of large strains in the soil mass, which was considered in other works recently presented in the literature, see e.g. [16,17].

First, the equations governing the dynamic flow of a liquid within a deformable porous medium are recalled and are coupled with those governing the deformation of its skeleton. Then they are re-written in finite element form. These derivations are pre-sented in some detail to allow the interested reader to follow their various steps.

On these bases two alternative finite element formulations are described. The first one does not introduce further assumptions with respect to those on which the governing equations are based. In this case the nodal variables consist of the displacements for the solid phase and of the relative seepage velocity for the liquid phase.

* Corresponding author. Tel.: +39 02 2399 4331; fax: +39 02 2399 4220.
E-mail addresses: annamaria.cividini@polimi.it (A. Cividini), giancarlo.gioda@polimi.it (G. Gioda).
[1] Tel.: +39 02 2399 4329; fax: +39 02 2399 4220.

©2015. This manuscript version is made available under the CC-BY-NC-ND 4.0 license http://creativecommons.org/licenses/by-nc-nd/4.0/
Published Journal Article available at: http://dx.doi.org/10.1016/j.compgeo.2015.11.017

Note that other formulations presented in the literature, e.g. [10,12], adopt as independent variables the displacements of both solid and liquid phases.

The second formulation represents a simplified approach which reduces the nodal variables to the displacements of the solid phase only.

An iterative time integration scheme is then outlined for both formulations and is applied in the solution of a test problem. The numerical results suggest some observations on the advantages and drawbacks of the two approaches in term of accuracy and computational effort.

In the following, the problem is approached considering the saturated porous medium equivalent to two superimposed continua, referred to as solid and liquid phases. The two phases have the same volume, which coincides with that of porous medium. This assumption involves the use of equivalent quantities that will be defined subsequently.

A matrix notation and an Eulerian approach with a constant geometry are adopted in this paper. All variables are in general functions of time t. Upper and lower case bold face letters denote matrices and column vectors, respectively. A superposed dot and a superscript T denote time derivative and transpose.

2. Equations governing the seepage flow

The dynamic equations governing the seepage flow of a liquid within a fully saturated porous skeleton are recalled here introducing some assumptions that seem reasonable in the geotechnical context. In particular, a Newtonian pore liquid is considered, referred to in the following as water, with constant deviatoric viscosity and no volumetric viscosity; this liquid has a constant density and its volumetric deformation linearly depends on the pore pressure; isothermal conditions are assumed, thus neglecting the influence of temperature; the fluid flow is laminar.

Let introduce now the following quantities: $\boldsymbol{v}_W$ is the vector collecting the Cartesian components of the velocity of the water particles; $\boldsymbol{v}$ represents the discharge velocity of flow in Darcy sense, which pertains to the liquid phase; $\dot{\boldsymbol{u}}$ is the velocity of the solid phase, which coincides with that of the soil skeleton; $\boldsymbol{w}_W$ is the relative velocity of the water particles with respect to the skeleton and $\boldsymbol{w}$ is the relative discharge velocity. The following relationships hold between these variables.

$$\boldsymbol{w}_W = \boldsymbol{v}_W - \dot{\boldsymbol{u}}, \quad \boldsymbol{w} = \boldsymbol{v} - \dot{\boldsymbol{u}} \tag{1a, b}$$

The relative discharge velocity $\boldsymbol{w}$ depends on the relative velocity of the water particles $\boldsymbol{w}_W$ through the matrix $\boldsymbol{N}_A$ of the area porosities.

$$\boldsymbol{w} = \boldsymbol{N}_A \boldsymbol{w}_W \tag{2}$$

If the principal directions of porosity coincide with the Cartesian axes, $\boldsymbol{N}_A$ is a 3×3 diagonal matrix the entries of which n_{Ax}, n_{Ay} and n_{Az} are the ratios between the area of pores and the total area of the sections normal to the reference axes.

The difficulties met in determining the area porosities suggest using the volume (or effective) porosity n, which represents the ratio between the volume of voids and the total volume of a soil element, and that can be seen as the average value of the area porosities [7]. Consequently, Eq. (2) becomes.

$$\boldsymbol{w} = n \boldsymbol{w}_W \tag{3}$$

2.1. Equation of compatibility

The equation of compatibility of the liquid phase relates its strain rates, collected in vector $\dot{\boldsymbol{\varepsilon}}_L$, to the discharge velocity $\boldsymbol{v}$ through the same 6x3 differential operator $\boldsymbol{B}$ (see the List of Symbols) that governs the strain–displacement relationship for solids.

$$\dot{\boldsymbol{\varepsilon}}_L = \boldsymbol{B}\boldsymbol{v} \tag{4}$$

Considering Eq. (1b), the relationship between the strain rate of the liquid phase $\dot{\boldsymbol{\varepsilon}}_L$, the relative discharge velocity $\boldsymbol{w}$ and the skeleton velocity $\dot{\boldsymbol{u}}$ is.

$$\dot{\boldsymbol{\varepsilon}}_L = \boldsymbol{B}\boldsymbol{w} + \boldsymbol{B}\dot{\boldsymbol{u}} \tag{5}$$

2.2. Shear stress-shear strain rate relationship

The stresses $\boldsymbol{\sigma}_L$ and the strain rates $\dot{\boldsymbol{\varepsilon}}_L$ of the liquid phase are expressed through the following quantities,

$$p = \frac{1}{3}\boldsymbol{m}^T\boldsymbol{\sigma}_L; \quad \boldsymbol{\tau}_L = \boldsymbol{\sigma}_L - \boldsymbol{m}p = \left(\boldsymbol{I} - \frac{1}{3}\boldsymbol{m}\boldsymbol{m}^T\right)\boldsymbol{\sigma}_L \tag{6a, b}$$

$$\dot{\varepsilon}_{L,vol} = \boldsymbol{m}^T\dot{\boldsymbol{\varepsilon}}_L; \quad \dot{\boldsymbol{e}}_L = \dot{\boldsymbol{\varepsilon}}_L - \frac{1}{3}\boldsymbol{m}\dot{\varepsilon}_{L,vol} = \left(\boldsymbol{I} - \frac{1}{3}\boldsymbol{m}\boldsymbol{m}^T\right)\dot{\boldsymbol{\varepsilon}}_L \tag{7a, b}$$

where p is the pore pressure (positive if tensile), which coincides with the volumetric part of the stresses $\boldsymbol{\sigma}_L$; $\boldsymbol{\tau}_L$ is the deviatoric stress vector; $\dot{\varepsilon}_{L,vol}$ and $\dot{\boldsymbol{e}}_L$ are the volumetric and deviatoric strain rates; $\boldsymbol{I}$ is the identity matrix and $\boldsymbol{m}$ is a 6 component vector the entries of which are equal to 1 if they correspond to normal strains/stresses, otherwise they vanish.

In a Newtonian liquid, a linear relationship holds between stresses and strain rates which is formally analogous to that relating stresses and strains for a linearly elastic solid. In the case of solids the law depends on bulk and shear elastic moduli; in the case of liquids on bulk and shear viscosities. Since the bulk viscosity is neglected in the present context, only the deviatoric part of the law remains.

$$\boldsymbol{\tau}_L = \mu_L \boldsymbol{I}_0 \dot{\boldsymbol{e}}_L \tag{8}$$

Here μ_L is the deviatoric viscosity of the liquid phase and $\boldsymbol{I}_0$ is a 6×6 diagonal matrix with entries equal to 2 if they correspond to normal strains, otherwise they are equal to 1.

Eqs. (8), (7) and (5) lead to the following $\boldsymbol{\tau}_L - \boldsymbol{w}$ relationship,

$$\boldsymbol{\tau}_L = \mu_L \boldsymbol{I}_1(\boldsymbol{B}\boldsymbol{w} + \boldsymbol{B}\dot{\boldsymbol{u}}) \tag{9}$$

where

$$\boldsymbol{I}_1 = \boldsymbol{I}_0 - \frac{1}{3}\boldsymbol{I}_0\boldsymbol{m}\boldsymbol{m}^T = \boldsymbol{I}_0 - \frac{2}{3}\boldsymbol{m}\boldsymbol{m}^T \tag{10}$$

Substituting Eq. (9) into Eq. (6b) one obtains.

$$\boldsymbol{\sigma}_L = \mu_L \boldsymbol{I}_1(\boldsymbol{B}\boldsymbol{w} + \boldsymbol{B}\dot{\boldsymbol{u}}) + \boldsymbol{m}p \tag{11}$$

2.3. Conservation of the mass of liquid

If internal sources are neglected, the conservation condition requires that the liquid phase mass, $\dot{m}_1$, accumulated in a unit volume in a unit time coincides with the difference, $\dot{m}_2$, between the rates of mass entering and leaving it.

$$\dot{m}_1 = \dot{m}_2 \tag{12}$$

The rate of mass accumulation, $\dot{m}_1$, consists of four contributions. The first one depends on the volumetric strain rate of the skeleton, $\dot{\varepsilon}_{S,vol}$, which in turn is a function of its displacement rate $\dot{\boldsymbol{u}}$.

$$\dot{\varepsilon}_{S,vol} = \boldsymbol{m}^T(\boldsymbol{B}\dot{\boldsymbol{u}}) \tag{13}$$

Since positive volume strains correspond to a volume increase, a positive value of $\dot{\varepsilon}_{S,vol}$ involves an increase of the liquid mass within the volume.

The second contribution is the change in mass due to the volumetric strain rate of the fluid phase that, disregarding its volumetric viscosity, depends on the pore pressure rate $\dot{p}$ through the bulk modulus B_W of the liquid and the volume porosity n.

The third contribution is due to the strain rate of the soil grains that depends on the pore pressure change through the bulk modulus of the soil grains B_G and on the porosity n.

Since tensile pore pressure are assumed as positive, a positive pore pressure rate corresponds to a volume increase of grains and water and, hence, to a decrease of the liquid mass.

The forth contribution, due to the change in density of the liquid, is here neglected. Hence, the rate of liquid mass accumulation is,

$$\dot{m}_1 = \rho_L \boldsymbol{m}^T(\boldsymbol{B}\dot{\boldsymbol{u}}) - \rho_L \frac{n}{B_W}\dot{p} - \rho_L \frac{1-n}{B_G}\dot{p} \tag{14}$$

where the density of the liquid phase ρ_L depends on that of water ρ_W and on n.

$$\rho_L = n\rho_W \tag{15}$$

The difference, $\dot{m}_2$, between the rates of liquid mass leaving and entering the volume depends on the space variations of the relative discharge velocity.

$$\dot{m}_2 = -\rho_L\left[\frac{\partial w_x}{\partial x} + \frac{\partial w_y}{\partial y} + \frac{\partial w_z}{\partial z}\right] = -\rho_L \boldsymbol{m}^T(\boldsymbol{B}\boldsymbol{w}) \tag{16}$$

Note that positive values of the space derivatives imply that the mass leaving the element exceeds the one entering it. Consequently, since $\dot{m}_2$ represents a mass accumulation, positive derivatives correspond to negative $\dot{m}_2$.

Substituting Eqs. (14) and (16) into Eq. (12), the conservation of the liquid mass for a three dimensional seepage flow becomes,

$$\boldsymbol{m}^T(\boldsymbol{B}\dot{\boldsymbol{u}}) + \boldsymbol{m}^T(\boldsymbol{B}\boldsymbol{w}) - \frac{1}{B_U}\dot{p} = 0 \tag{17}$$

where B_U is the parameter that governs the change in volume of the saturated porous medium, which depends on the bulk moduli of water B_W and grains B_G.

$$B_U = \left(\frac{n}{B_W} + \frac{1-n}{B_G}\right)^{-1} \tag{18}$$

2.4. Equation of motion of the fluid phase

Adopting an Eulerian approach for the liquid flow, the equation of motion expresses the momentum balance of the mass contained within a fixed unit volume. This implies that the rate of momentum increase is equal to the difference between the inward and outward momentum rates plus the contribution of the external forces.

The equation of motion for a one dimensional flow of the liquid phase in the x direction reads,

$$\rho_L \frac{\partial v_x}{\partial t} + \rho_L\left[\frac{\partial (v_x v_x)}{\partial x} + \frac{\partial (v_x v_y)}{\partial y} + \frac{\partial (v_x v_z)}{\partial z}\right] - \left(\frac{\partial \sigma_{Lx}}{\partial x} + \frac{\partial \tau_{Lyx}}{\partial y} + \frac{\partial \tau_{Lzx}}{\partial z}\right) - \rho_L \overline{g}_x + f_{Dx} = 0 \tag{19}$$

where ρ_L is the density of the liquid phase (Eq. (15)); v_i $(i = x, y, z)$ are the components of the discharge velocity; σ_{Lx}, τ_{Lyx}, τ_{Lzx} are normal and shear stress components of the liquid phase; $\overline{g}_x$ is the component of the acceleration of gravity in the x direction and f_{Dx} is the drag force due the interaction between the flowing liquid and the porous skeleton. Note that while the acceleration of gravity is known and constant with time, the discharge velocity and its time derivative are unknown quantities.

Writing Eq. (19) for a three dimensional seepage flow, expressing the discharge velocity $\boldsymbol{v}$ in terms of the relative discharge velocity $\boldsymbol{w}$ and of the skeleton velocity $\dot{\boldsymbol{u}}$ through Eq. (1b), and neglecting the quadratic term because the small value of velocity makes its contribution marginal in geotechnical seepage problems, one obtains.

$$\rho_L \dot{\boldsymbol{w}} + \rho_L \ddot{\boldsymbol{u}} - \boldsymbol{B}^T \boldsymbol{\sigma}_L - \rho_L \overline{\boldsymbol{g}} + \boldsymbol{f}_D = \boldsymbol{0} \tag{20}$$

Here vectors $\dot{\boldsymbol{w}}$, $\ddot{\boldsymbol{u}}$, $\overline{\boldsymbol{g}}$ and $\boldsymbol{f}_D$ collect, respectively, the components of: relative discharge acceleration; skeleton acceleration; acceleration of gravity (which is known and constant with time) and drag force.

Confining our attention to laminar flows, the following relationship can be introduced between the drag force vector and the relative discharge velocity.

$$\boldsymbol{f}_D = \mu_L (\boldsymbol{K}')^{-1} \boldsymbol{w} \tag{21}$$

In the above equation $\boldsymbol{K}'$ is the intrinsic permeability matrix of the porous skeleton and μ_L is the deviatoric viscosity of the liquid phase. Note that under gravity conditions the relationship between the intrinsic permeability k' (having dimensions of square length) and the coefficient of permeability k (having dimensions of velocity) is,

$$k = \frac{\gamma_W}{\mu_W} k' \tag{22}$$

where γ_W and μ_W are the unit weight and the viscosity of water.

Finally, expressing $\boldsymbol{\sigma}_L$ and $\boldsymbol{f}_D$ in Eq. (20) through Eqs. (11) and (21), the matrix form of the equation of motion of the fluid phase is arrived at.

$$\rho_L \dot{\boldsymbol{w}} + \rho_L(\ddot{\boldsymbol{u}} - \overline{\boldsymbol{g}}) - \mu_L \boldsymbol{B}^T[\boldsymbol{I}_1 \boldsymbol{B}(\boldsymbol{w})] - \mu_L \boldsymbol{B}^T[\boldsymbol{I}_1 \boldsymbol{B}(\dot{\boldsymbol{u}})] - \boldsymbol{B}^T(\boldsymbol{m}p) + \mu_L (\boldsymbol{K}')^{-1}\boldsymbol{w} = \boldsymbol{0} \tag{23}$$

3. Governing equations for the two-phase medium

In one dimensional condition, and neglecting the quadratic velocity terms, the equation of motion for the two-phase medium is,

$$\rho_S \ddot{u}_x + \rho_L \frac{\partial v_x}{\partial t} - \left(\frac{\partial \sigma_x}{\partial x} + \frac{\partial \tau_{yx}}{\partial y} + \frac{\partial \tau_{zx}}{\partial z}\right) - (\rho_S + \rho_L)\overline{g}_x = 0 \tag{24}$$

where v_x is the velocity of the liquid phase, $\ddot{u}_x$ is the skeleton acceleration, ρ_S and ρ_L are the (constant) densities of solid and liquid phases, and σ_x, τ_{yx}, τ_{zx} are normal (positive if tensile) and shear total stress components.

Taking into account Eq. (1b), for a three dimensional motion Eq. (24) becomes.

$$\rho_{Sat} \ddot{\boldsymbol{u}} + \rho_L \dot{\boldsymbol{w}} - \boldsymbol{B}^T \boldsymbol{\sigma} - \rho_{Sat} \overline{\boldsymbol{g}} = \boldsymbol{0} \tag{25}$$

Here ρ_{Sat} represents the density of the saturated porous medium, which depends on the densities of soil grains ρ_G and water ρ_W and on the porosity n.

$$\rho_{Sat} = \rho_S + \rho_L = (1-n)\rho_G + n\rho_W \tag{26}$$

The vector of total stresses $\boldsymbol{\sigma}$ is expressed in terms of the stresses acting on the solid phase, $\boldsymbol{\sigma}'_S$, and on the liquid phase, $\boldsymbol{\sigma}_L$.

$$\boldsymbol{\sigma} = \boldsymbol{\sigma}'_S + \boldsymbol{\sigma}_L \tag{27}$$

Biot's coefficient α [18], which affects the isotropic part of $\boldsymbol{\sigma}_L$ (i.e. the pore pressure), has been omitted in Eq. (27) since its value is close to unity in the case of granular soils here considered.

In the small strain regime, and assuming that in dynamic conditions the skeleton behavior can be reasonably expressed by uncoupling the effects of strain from those of the strain rate, the following relationships hold.

$$\boldsymbol{\varepsilon}_S = \boldsymbol{B}\boldsymbol{u} \tag{28}$$

$$\boldsymbol{\sigma}'_S = \boldsymbol{D}_S\boldsymbol{\varepsilon}_S + \boldsymbol{V}_S\dot{\boldsymbol{\varepsilon}}_S \tag{29}$$

Here vector $\boldsymbol{\varepsilon}_S$ collects the strain components of the solid phase and $\boldsymbol{D}_S$ and $\boldsymbol{V}_S$ are its constitutive elastic and viscosity matrices.

Introducing Eq. (27) into Eq. (25), and expressing the stress vectors $\boldsymbol{\sigma}'_S$ and $\boldsymbol{\sigma}_L$ through Eqs. (28), (29) and (11), one obtains,

$$\rho_{Sat}(\ddot{\boldsymbol{u}} - \overline{\boldsymbol{g}}) + \rho_L\dot{\boldsymbol{w}} - \boldsymbol{B}^T[\boldsymbol{D}_S\boldsymbol{B}(\boldsymbol{u})] - \boldsymbol{B}^T[\boldsymbol{V}_{SL}\boldsymbol{B}(\dot{\boldsymbol{u}})] - \mu_L\boldsymbol{B}^T[\boldsymbol{I}_1\boldsymbol{B}(\boldsymbol{w})] - \boldsymbol{B}^T(\boldsymbol{m}p) = \boldsymbol{0} \tag{30}$$

where $\boldsymbol{V}_{SL}$ is the global constitutive viscosity matrix of the coupled solid and liquid phases.

$$\boldsymbol{V}_{SL} = \boldsymbol{V}_S + n\mu_L\boldsymbol{I}_1 \tag{31}$$

4. Boundary conditions

The dynamic two-phase problem is governed by the system of three differential Eqs. (17), (23) and (30), which involve as unknown functions the relative discharge velocity $\boldsymbol{w}$, the skeleton displacements $\boldsymbol{u}$ and the pore pressure p.

To express the boundary conditions with reference to confined seepage flows, consider a saturated porous domain having surface Γ and volume Ω.

The surface Γ is subdivided into its impervious part, Γ_w, where the relative discharge velocity component normal to it, $\overline{w}_n$, vanishes and its pervious part, Γ_p, where the pore pressure $\overline{p}$ is known. The corresponding boundary conditions can be expressed as follows.

$$\boldsymbol{w}^T\boldsymbol{T}_1\boldsymbol{m} = \boldsymbol{m}^T\boldsymbol{T}_1^T\boldsymbol{w} = \overline{w}_n = 0 \text{ on } \Gamma_w \tag{32a}$$

$$p = \overline{p} \quad \text{and} \quad \boldsymbol{\tau}_{\boldsymbol{L}} = \boldsymbol{0} \text{ on } \Gamma_p \tag{32b, c}$$

In Eq. (32a) $\boldsymbol{T}_1$ is a 3×6 matrix the entries of which are the direction cosines of the outward vector normal to Γ_w (see List of Symbols).

The surface Γ can be also subdivided into Γ_u, where the displacements $\overline{\boldsymbol{u}}$ are known, and Γ_σ where the three components of the total surface tractions $\overline{\boldsymbol{t}}$ are imposed.

$$\boldsymbol{T}_2\boldsymbol{u} = \overline{\boldsymbol{u}} \text{ on } \Gamma_u \tag{32d}$$

$$\boldsymbol{T}_2\boldsymbol{T}_1\boldsymbol{\sigma} = \overline{\boldsymbol{t}} \text{ on } \Gamma_\sigma \tag{32e}$$

In Eq. (32d,e) T_2 is the 3×3 matrix containing the direction cosines of the local reference system axes along which the boundary displacements and tractions are imposed.

5. Finite element approximation

Consider the eth finite element adopted for discretizing the saturated porous medium and denote with n_w^e and n_u^e the number of its nodes where relative discharge velocity $\boldsymbol{w}^e$ and displacements $\boldsymbol{u}^e$ are defined, respectively. The pore pressure p^e is seen here as an element variable and is defined at the element integration points.

The distributions of the relative discharge velocities $\boldsymbol{w}$ and of the solid phase displacements $\boldsymbol{u}$ within the element depend on the interpolation function matrices $\boldsymbol{S}_w^e$ and $\boldsymbol{S}_u^e$.

$$\boldsymbol{w} = \boldsymbol{S}_w^e\boldsymbol{w}^e; \quad \boldsymbol{u} = \boldsymbol{S}_u^e\boldsymbol{u}^e \tag{33a, b}$$

For a three-dimensional problem, $\boldsymbol{S}_w^e$ is a $3 \times 3\ n_w^e$ matrix and $\boldsymbol{S}_u^e$ is a $3 \times 3\ n_u^e$ matrix. Let also define the following matrices containing the space derivatives of the interpolation functions, where $\boldsymbol{B}_w^e$ is a $6 \times 3\ n_w^e$ matrix and $\boldsymbol{B}_u^e$ is a $6 \times 3\ n_u^e$ matrix.

$$\boldsymbol{B}_w^e = \boldsymbol{B}\boldsymbol{S}_w^e; \quad \boldsymbol{B}_u^e = \boldsymbol{B}\boldsymbol{S}_u^e \tag{34a, b}$$

6. Finite element formulations

Two finite element formulations will be outlined in the following. The first one does not introduce further assumptions with respect to those already adopted for deriving the governing Eqs. (17), (23) and (30). In this case the nodal variables consist of the displacement $\boldsymbol{u}$ for the solid phase and of the relative seepage velocity $\boldsymbol{w}$ for the liquid phase. Note that other formulations previously presented in the literature (e.g. [10,12]) adopt as nodal variables the displacements of the solid and of the liquid phases.

An alternative, simplified formulation is described subsequently where the nodal variables are reduced to the displacements of the solid phase only.

6.1. Finite element form of Eq. (23)

To derive their finite element form, Eq. (23) and the boundary condition Eq. (32b) are written in weak form multiplying them by a virtual variation $\delta\boldsymbol{w}$ of the relative discharge velocity that ful-fils Eq. (32a) on Γ_w and integrating them, respectively, over the volume Ω and the surface Γ_p of an element of the porous medium.

$$\rho_L\int_\Omega \delta\boldsymbol{w}^T(\dot{\boldsymbol{w}} + \ddot{\boldsymbol{u}} - \overline{\boldsymbol{g}})d\Omega - \mu_L\int_\Omega \delta\boldsymbol{w}^T\boldsymbol{B}^T[\boldsymbol{I}_1(\boldsymbol{B}\boldsymbol{w})]d\Omega - \mu_L\int_\Omega \delta\boldsymbol{w}^T\boldsymbol{B}^T[\boldsymbol{I}_1(\boldsymbol{B}\dot{\boldsymbol{u}})]d\Omega - \int_\Omega \delta\boldsymbol{w}^T(\boldsymbol{B}^T\boldsymbol{m}p)d\Omega + \mu_L\int_\Omega \delta\boldsymbol{w}^T(\boldsymbol{K}')^{-1}\boldsymbol{w}d\Omega + \int_{\Gamma_p} \delta\boldsymbol{w}^T\boldsymbol{T}_1\boldsymbol{m}(p - \overline{p})d\Gamma = 0 \tag{35}$$

Applying Green–Gauss theorem (see Appendix A) to the second, third and fourth integrals in Eq. (35) one obtains, respectively.

$$-\mu_L\int_\Omega \delta\boldsymbol{w}^T\boldsymbol{B}^T[\boldsymbol{I}_1(\boldsymbol{B}\boldsymbol{w})]d\Omega = -\mu_L\int_{\Gamma_p} \delta\boldsymbol{w}^T\boldsymbol{T}_1\boldsymbol{I}_1(\boldsymbol{B}\boldsymbol{w})d\Gamma + \mu_L\int_\Omega (\boldsymbol{B}\delta\boldsymbol{w})^T\boldsymbol{I}_1(\boldsymbol{B}\boldsymbol{w})d\Omega \tag{36a}$$

$$-\mu_L\int_\Omega \delta\boldsymbol{w}^T\boldsymbol{B}^T[\boldsymbol{I}_1(\boldsymbol{B}\dot{\boldsymbol{u}})]d\Omega = -\mu_L\int_{\Gamma_p} \delta\boldsymbol{w}^T\boldsymbol{T}_1\boldsymbol{I}_1(\boldsymbol{B}\dot{\boldsymbol{u}})d\Gamma + \mu_L\int_\Omega (\boldsymbol{B}\delta\boldsymbol{w})^T\boldsymbol{I}_1(\boldsymbol{B}\dot{\boldsymbol{u}})d\Omega \tag{36b}$$

$$-\int_\Omega \delta\boldsymbol{w}^T(\boldsymbol{B}^T\boldsymbol{m}p)d\Omega = -\int_{\Gamma_p} \delta\boldsymbol{w}^T\boldsymbol{T}_1\boldsymbol{m}pd\Gamma + \int_\Omega (\boldsymbol{B}\delta\boldsymbol{w})^T\boldsymbol{m}pd\Omega \tag{36c}$$

Note that, since $\delta\boldsymbol{w}$ fulfils Eq. (32a), the surface integrals over the impervious surface Γ_w vanish. In addition, considering Eqs. (9) and (32c), the following equation holds.

$$-\mu_L\int_{\Gamma_p} \delta\boldsymbol{w}^T\boldsymbol{T}_1\boldsymbol{I}_1(\boldsymbol{B}\boldsymbol{w})d\Gamma = \mu_L\int_{\Gamma_p} \delta\boldsymbol{w}^T\boldsymbol{T}_1\boldsymbol{I}_1(\boldsymbol{B}\dot{\boldsymbol{u}})d\Gamma \tag{36d}$$

Substitution of Eqs. (36) into Eq. (35) leads to

$$\rho_L\int_\Omega \delta\boldsymbol{w}^T(\dot{\boldsymbol{w}} + \ddot{\boldsymbol{u}} - \overline{\boldsymbol{g}})d\Omega + \mu_L\int_\Omega (\boldsymbol{B}\delta\boldsymbol{w})^T\boldsymbol{I}_1(\boldsymbol{B}\boldsymbol{w})d\Omega + \mu_L\int_\Omega (\boldsymbol{B}\delta\boldsymbol{w})^T\boldsymbol{I}_1(\boldsymbol{B}\dot{\boldsymbol{u}})d\Omega + \mu_L\int_\Omega \delta\boldsymbol{w}^T(\boldsymbol{K}')^{-1}\boldsymbol{w}d\Omega = -\int_\Omega (\boldsymbol{B}\delta\boldsymbol{w})^T\boldsymbol{m}pd\Omega + \int_{\Gamma_p} \delta\boldsymbol{w}^T\boldsymbol{T}_1\boldsymbol{m}\overline{p}d\Gamma \tag{37}$$

Finally, the following set of n_W^e scalar equations is reached by writing Eq. (37) for the eth element, by introducing Eqs. (33) and (34) and by eliminating from all terms the virtual variation of the nodal discharge velocities.

$$\boldsymbol{M}^e_{Lww}\dot{\boldsymbol{w}}^e + \boldsymbol{M}^e_{Lwu}\ddot{\boldsymbol{u}}^e + \boldsymbol{V}^e_{Lww}\boldsymbol{w}^e + \boldsymbol{V}^e_{Lwu}\dot{\boldsymbol{u}}^e = \boldsymbol{f}^e_{Lp} + \bar{\boldsymbol{f}}^e_{Lp} + \bar{\boldsymbol{f}}^e_{Lg} \tag{38}$$

The following expressions hold for matrices and vectors in Eq. (38), where the subscript L indicates that they are related to the liquid phase and a superposed bar denotes the vectors of data.

$$\boldsymbol{M}^e_{Lww} = \rho_L \int_{\Omega^e} (\boldsymbol{S}^e_w)^T \boldsymbol{S}^e_w d\Omega; \quad \boldsymbol{M}^e_{Lwu} = \rho_L \int_{\Omega^e} (\boldsymbol{S}^e_w)^T \boldsymbol{S}^e_u d\Omega \tag{39a, b}$$

$$\begin{aligned}\boldsymbol{V}^e_{Lww} &= \boldsymbol{V}^e_{Lww1} + \boldsymbol{V}^e_{Lww2} \\ &= \mu_L \int_{\Omega^e} (\boldsymbol{B}^e_w)^T \boldsymbol{I}_1 \boldsymbol{B}^e_w d\Omega + \mu_L \int_{\Omega^e} (\boldsymbol{S}^e_w)^T (\boldsymbol{K}')^{-1} \boldsymbol{S}^e_w d\Omega;\end{aligned} \tag{39c}$$

$$\boldsymbol{V}^e_{Lwu} = \mu_L \int_{\Omega^e} (\boldsymbol{B}^e_w)^T \boldsymbol{I}_1 \boldsymbol{B}^e_u d\Omega; \quad \boldsymbol{f}^e_{Lp} = \int_{\Omega^e} (\boldsymbol{B}^e_w)^T \boldsymbol{m} p^e d\Omega \tag{39d, e}$$

$$\bar{\boldsymbol{f}}^e_{Lp} = \int_{\Gamma^e_p} (\boldsymbol{S}^e_w)^T \boldsymbol{T}_1 \boldsymbol{m} \bar{p}^e d\Gamma; \quad \bar{\boldsymbol{f}}^e_{Lg} = \rho_L \int_{\Omega^e} (\boldsymbol{S}^e_w)^T \bar{\boldsymbol{g}} d\Omega; \tag{39f, g}$$

Note that vector $\boldsymbol{f}^e_{Lp}$ (Eq. (39e)) depends on the unknown pore pressure distribution within the element.

6.2. Finite element form of Eq. (30)

Eq. (30) and the boundary condition Eq. (32e) are written in weak form multiplying them by a virtual variation of the displacements $\delta\boldsymbol{u}$ of the solid phase that fulfils Eq. (32d) on Γ_u and integrating them, respectively, over Ω and Γ_σ.

$$\begin{aligned}&\int_\Omega \delta\boldsymbol{u}^T[\rho_{Sat}(\ddot{\boldsymbol{u}} - \bar{\boldsymbol{g}}) + \rho_L \dot{\boldsymbol{w}}]d\Omega - \int_\Omega \delta\boldsymbol{u}^T \boldsymbol{B}^T[\boldsymbol{D}_S(\boldsymbol{B}\boldsymbol{u})]d\Omega \\ &- \int_\Omega \delta\boldsymbol{u}^T \boldsymbol{B}^T[\boldsymbol{V}_{SL}(\boldsymbol{B}\dot{\boldsymbol{u}})]d\Omega - \mu_L \int_\Omega \delta\boldsymbol{u}^T \boldsymbol{B}^T[\boldsymbol{I}_1(\boldsymbol{B}\boldsymbol{w})]d\Omega \\ &- \int_\Omega \delta\boldsymbol{u}^T(\boldsymbol{B}^T\boldsymbol{m}p)d\Omega + \int_{\Gamma_\sigma} \delta\boldsymbol{u}^T \boldsymbol{T}_2^T(\boldsymbol{T}_2\boldsymbol{T}_1\boldsymbol{\sigma} - \bar{\boldsymbol{t}})d\Gamma = 0\end{aligned} \tag{40}$$

Applying Green–Gauss theorem (see Appendix A) to the second, third, fourth and fifth integrals in Eq. (40) one obtains, respectively.

$$\begin{aligned}&-\int_\Omega \delta\boldsymbol{u}^T \boldsymbol{B}^T[\boldsymbol{D}_S(\boldsymbol{B}\boldsymbol{u})]d\Omega = -\int_{\Gamma_\sigma} \delta\boldsymbol{u}^T \boldsymbol{T}_1 \boldsymbol{D}_S(\boldsymbol{B}\boldsymbol{u})d\Gamma \\ &+\int_\Omega (\boldsymbol{B}\delta\boldsymbol{u})^T \boldsymbol{D}_S(\boldsymbol{B}\boldsymbol{u})d\Omega\end{aligned} \tag{41a}$$

$$\begin{aligned}&-\int_\Omega \delta\boldsymbol{u}^T \boldsymbol{B}^T[\boldsymbol{V}_{SL}(\boldsymbol{B}\dot{\boldsymbol{u}})]d\Omega = -\int_{\Gamma_\sigma} \delta\boldsymbol{u}^T \boldsymbol{T}_1 \boldsymbol{V}_{SL}(\boldsymbol{B}\dot{\boldsymbol{u}})d\Gamma \\ &+\int_\Omega (\boldsymbol{B}\delta\boldsymbol{u})^T \boldsymbol{V}_{SL}(\boldsymbol{B}\dot{\boldsymbol{u}})d\Omega\end{aligned} \tag{41b}$$

$$\begin{aligned}&-\mu_L\int_\Omega \delta\boldsymbol{u}^T \boldsymbol{B}^T[\boldsymbol{I}_1(\boldsymbol{B}\boldsymbol{w})]d\Omega = -\mu_L\int_{\Gamma_\sigma} \delta\boldsymbol{u}^T \boldsymbol{T}_1 \boldsymbol{I}_1(\boldsymbol{B}\boldsymbol{w})]d\Gamma \\ &+\mu_L\int_\Omega (\boldsymbol{B}\delta\boldsymbol{u})^T \boldsymbol{I}_1(\boldsymbol{B}\boldsymbol{w})d\Omega\end{aligned} \tag{41c}$$

$$-\int_\Omega \delta\boldsymbol{u}^T(\boldsymbol{B}^T\boldsymbol{m}p)d\Omega = -\int_{\Gamma_\sigma} \delta\boldsymbol{u}^T \boldsymbol{T}_1 \boldsymbol{m} p d\Gamma + \int_\Omega (\boldsymbol{B}\delta\boldsymbol{u})^T \boldsymbol{m} p d\Omega \tag{41d}$$

Note that the surface integrals over Γ_u in Eqs. (41) vanish (cf. Eq. (32d)) and that, taking into account Eqs. (27)–(29), (11), the last integral over Γ_σ in Eq. (40) becomes.

$$\begin{aligned}\int_{\Gamma_\sigma} \delta\boldsymbol{u}^T \boldsymbol{T}_2^T(\boldsymbol{T}_2\boldsymbol{T}_1\boldsymbol{\sigma} - \bar{\boldsymbol{t}})d\Gamma &= \int_{\Gamma_\sigma} \delta\boldsymbol{u}^T \boldsymbol{T}_1 \boldsymbol{D}_S(\boldsymbol{B}\boldsymbol{u})d\Gamma \\ &+ \int_{\Gamma_\sigma} \delta\boldsymbol{u}^T \boldsymbol{T}_1 \boldsymbol{V}_S(\boldsymbol{B}\dot{\boldsymbol{u}})d\Gamma \\ &+ \mu_L \int_{\Gamma_\sigma} \delta\boldsymbol{u}^T \boldsymbol{T}_1 \boldsymbol{I}_1(\boldsymbol{B}\boldsymbol{w})d\Gamma \\ &+ n\mu_L \int_{\Gamma_\sigma} \delta\boldsymbol{u}^T \boldsymbol{T}_1 \boldsymbol{I}_1(\boldsymbol{B}\dot{\boldsymbol{u}})]d\Gamma \\ &+ \int_{\Gamma_\sigma} \delta\boldsymbol{u}^T \boldsymbol{T}_1 \boldsymbol{m} p d\Gamma \\ &- \int_{\Gamma_\sigma} \delta\boldsymbol{u}^T \boldsymbol{T}_2^T \bar{t} d\Gamma\end{aligned} \tag{41e}$$

Substitution of Eqs. (41) and (31) into Eq. (40) leads to.

$$\begin{aligned}&\int_\Omega \delta\boldsymbol{u}^T[\rho_{Sat}(\ddot{\boldsymbol{u}} - \bar{\boldsymbol{g}}) + \rho_L \dot{\boldsymbol{w}}]d\Omega + \int_\Omega (\boldsymbol{B}\delta\boldsymbol{u})^T \boldsymbol{D}_S(\boldsymbol{B}\boldsymbol{u})d\Omega \\ &+ \int_\Omega (\boldsymbol{B}\delta\boldsymbol{u})^T \boldsymbol{V}_{SL}(\boldsymbol{B}\dot{\boldsymbol{u}})d\Omega + \mu_L \int_\Omega (\boldsymbol{B}\delta\boldsymbol{u})^T \boldsymbol{I}_1(\boldsymbol{B}\boldsymbol{w})d\Omega \\ &= \int_{\Gamma_\sigma} \delta\boldsymbol{u}^T \boldsymbol{T}_2^T \bar{\boldsymbol{t}} d\Gamma - \int_\Omega (\boldsymbol{B}\delta\boldsymbol{u})^T \boldsymbol{m} p d\Omega\end{aligned} \tag{42}$$

6.3. Displacement-velocity approach

Writing Eq. (42) for the eth element, introducing the interpolation functions and their derivatives (Eqs. (33) and (34)), and eliminating from all terms the virtual variation of the nodal displacements, the following matrix form is arrived at, which corresponds to n^e_u scalar equations.

$$\begin{aligned}&\boldsymbol{K}^e_S \boldsymbol{u}^e + \boldsymbol{V}^e_{Sat}\dot{\boldsymbol{u}}^e + \boldsymbol{M}^e_{Sat}\ddot{\boldsymbol{u}}^e + (\boldsymbol{V}^e_{Lwu})^T \boldsymbol{w}^e + (\boldsymbol{M}^e_{Lwu})^T \dot{\boldsymbol{w}}^e \\ &= -\boldsymbol{f}^e_{up} + \bar{\boldsymbol{f}}^e_{gSat} + \bar{\boldsymbol{f}}^e_t\end{aligned} \tag{43}$$

Matrices $\boldsymbol{M}^e_{Lwu}$ and $\boldsymbol{V}^e_{Lwu}$ are given by Eqs. (39b,d). The stiffness matrix $\boldsymbol{K}^e_S$ of the solid element, the viscosity $\boldsymbol{V}^e_{Sat}$ and mass $\boldsymbol{M}^e_{Sat}$ matrices of the saturated two-phase element, and the vectors in Eq. (43) have the following expressions.

$$\boldsymbol{K}^e_S = \int_{\Omega^e} (\boldsymbol{B}^e_u)^T \boldsymbol{D}_S \boldsymbol{B}^e_u d\Omega; \quad \boldsymbol{V}^e_{Sat} = \int_{\Omega^e} (\boldsymbol{B}^e_u)^T \boldsymbol{V}_{SL} \boldsymbol{B}^e_u d\Omega \tag{44a, b}$$

$$\boldsymbol{M}^e_{Sat} = \rho_{Sat} \int_{\Omega^e} (\boldsymbol{S}^e_u)^T \boldsymbol{S}^e_u d\Omega; \quad \boldsymbol{f}^e_{up} = \int_{\Omega^e} (\boldsymbol{B}^e_u)^T \boldsymbol{m} p^e d\Omega \tag{44c, d}$$

$$\bar{\boldsymbol{f}}^e_{gSat} = \rho_{Sat} \int_{\Omega^e} (\boldsymbol{S}^e_u)^T \bar{\boldsymbol{g}} d\Omega; \quad \bar{\boldsymbol{f}}^e_t = \int_{\Omega^e} (\boldsymbol{S}^e_u) \boldsymbol{T}_2^T \bar{\boldsymbol{t}}^e d\Omega \tag{44e, f}$$

Note that vector $\boldsymbol{f}^e_{up}$ (Eq. (44d)) depends on the unknown pore pressure distribution within the element.

The final set of solving equation consists of Eqs. (43) and (38), which are re-written here for convenience.

$$\begin{aligned}&\begin{bmatrix}\boldsymbol{K}^e_S & \boldsymbol{0} \\ \boldsymbol{0} & \boldsymbol{0}\end{bmatrix}\begin{Bmatrix}\boldsymbol{u}^e \\ \boldsymbol{0}\end{Bmatrix} + \begin{bmatrix}\boldsymbol{V}^e_{Sat} & (\boldsymbol{V}^e_{Lwu})^T \\ \boldsymbol{V}^e_{Lwu} & \boldsymbol{V}^e_{Lww}\end{bmatrix}\begin{Bmatrix}\dot{\boldsymbol{u}}^e \\ \boldsymbol{w}^e\end{Bmatrix} \\ &+ \begin{bmatrix}\boldsymbol{M}^e_{Sat} & (\boldsymbol{M}^e_{Lwu})^T \\ \boldsymbol{M}^e_{Lwu} & \boldsymbol{M}^e_{Lww}\end{bmatrix}\begin{Bmatrix}\ddot{\boldsymbol{u}}^e \\ \dot{\boldsymbol{w}}^e\end{Bmatrix} = \begin{Bmatrix}-\boldsymbol{f}^e_{up} \\ \boldsymbol{f}^e_{Lp}\end{Bmatrix} + \begin{Bmatrix}\bar{\boldsymbol{f}}^e_{gSat} + \bar{\boldsymbol{f}}^e_t \\ \bar{\boldsymbol{f}}^e_{Lp} + \bar{\boldsymbol{f}}^e_{Lg}\end{Bmatrix}\end{aligned} \tag{45}$$

Having evaluated the nodal velocities of the solid and liquid phases, the pore pressure rate within the eth element is determined through Eq. (46) that represents the finite element form of Eq. (17).

$$\dot{p}^e = B_U(\boldsymbol{m}^T \boldsymbol{B}^e_u \dot{\boldsymbol{u}}^e + \boldsymbol{m}^T \boldsymbol{B}^e_w \boldsymbol{w}^e) \tag{46}$$

6.4. Displacement approach

An alternative formulation [12], which does not involve the discharge velocity as an independent variable, takes into account that some terms of Eq. (23) can be disregarded since their contribution is likely to be marginal with respect to that of other terms. These are the first term of Eq. (23), which depends on the relative discharge acceleration, and the third and fourth terms that contain the second space derivatives of the discharge velocity and of the velocity of the solid phase.

Based on the above assumptions, Eq. (23) reduces to the following form,

$$\boldsymbol{w} = \frac{1}{\mu_L}\boldsymbol{K}'[\boldsymbol{B}^T(\boldsymbol{m}p) - \rho_L(\ddot{\boldsymbol{u}} - \overline{\boldsymbol{g}})] \tag{47a}$$

which for the eth finite element becomes.

$$\boldsymbol{w}^e = [\boldsymbol{V}^e_{Lww2}]^{-1}[\boldsymbol{f}^e_{Lp} + \overline{\boldsymbol{f}}^e_{Lp} + \overline{\boldsymbol{f}}^e_{Lg} - \boldsymbol{M}^e_{Lwu}\ddot{\boldsymbol{u}}^e] \tag{47b}$$

Consider now Eq. (30) that, neglecting the discharge acceleration and the second space derivative of the discharge velocity, becomes.

$$\rho_{Sat}(\ddot{\boldsymbol{u}} - \overline{\boldsymbol{g}}) - \boldsymbol{B}^T[\boldsymbol{D}_S(\boldsymbol{B}\boldsymbol{u})] - \boldsymbol{B}^T[\boldsymbol{V}_{SL}(\boldsymbol{B}\dot{\boldsymbol{u}})] - \boldsymbol{B}^T(\boldsymbol{m}p) = \boldsymbol{0} \tag{48}$$

Consequently, its finite element form expressed by Eq. (43) reduces to.

$$\boldsymbol{K}^e_S\boldsymbol{u}^e + \boldsymbol{V}^e_{Sat}\dot{\boldsymbol{u}}^e + \boldsymbol{M}^e_{Sat}\ddot{\boldsymbol{u}}^e = -\boldsymbol{f}^e_{up} + \overline{\boldsymbol{f}}^e_{gSat} + \overline{\boldsymbol{f}}^e_t \tag{49}$$

Having evaluated the nodal velocities of the solid phase by Eq. (49), the velocity of the liquid phase and the pore pressure rate are determined through Eqs. (47b) and (46).

7. Time integration scheme

Let write Eqs. (45) and (49) of the two formulations in the same compact form expressed by Eq. (50), with obvious meanings of symbols.

$$\boldsymbol{Z}_1\boldsymbol{x}(t) + \boldsymbol{Z}_2\dot{\boldsymbol{x}}(t) + \boldsymbol{Z}_3\ddot{\boldsymbol{x}}(t) = \boldsymbol{b}(p,t) + \overline{\boldsymbol{b}}(t) \tag{50}$$

Note that vector $\boldsymbol{b}$ depends on the pore pressure, while $\overline{\boldsymbol{b}}$ is known and depends solely on time t.

To integrate Eq. (50) in time, assume that the variation of $\ddot{\boldsymbol{x}}(t)$ within a time increment Δt_i is governed by an a priori chosen interpolation function [19–22]. Consequently, the following equations express the independent variable and its first time derivative at the end of the interval $\Delta t_i = t_i - t_{i-1}$.

$$\boldsymbol{x}_i = \boldsymbol{x}_{i-1} + \int_{t(i-1)}^{t(i)} \dot{\boldsymbol{x}}(t)dt; \quad \dot{\boldsymbol{x}}_i = \dot{\boldsymbol{x}}_{i-1} + \int_{t(i-1)}^{t(i)} \ddot{\boldsymbol{x}}(t)dt \tag{51a,b}$$

Upon integration, Eqs. (51) can be written in the following form

$$\boldsymbol{x}_i = \left[\boldsymbol{x}_{i-1} + \Delta t_i\dot{\boldsymbol{x}}_{i-1} + \frac{\Delta t_i^2}{2}\ddot{\boldsymbol{x}}_{i-1}\right] + \beta_0\frac{\Delta t_i^2}{2}\Delta\ddot{\boldsymbol{x}}_i;$$
$$\dot{\boldsymbol{x}}_i = [\dot{\boldsymbol{x}}_{i-1} + \Delta t_i\ddot{\boldsymbol{x}}_{i-1}] + \beta_1\Delta t_i\Delta\ddot{\boldsymbol{x}}_i \tag{52a,b}$$

and

$$\ddot{\boldsymbol{x}}_i = \ddot{\boldsymbol{x}}_{i-1} + \Delta\ddot{\boldsymbol{x}}_i \tag{52c}$$

where $\Delta\ddot{\boldsymbol{x}}_i$ represents the increment of the second derivative at the end of the step.

The coefficients β_0 and β_1 depend on the interpolation function adopted for $\ddot{\boldsymbol{x}}(t)$ within the time step Δt_i. In particular, $\beta_0 = 1$ and $\beta_1 = 0$ if $\ddot{\boldsymbol{x}}(t) = \ddot{\boldsymbol{x}}_i$; $\beta_0 = \beta_1 = 1/2$ if $\ddot{\boldsymbol{x}}(t) = (\ddot{\boldsymbol{x}}_{i-1} + \ddot{\boldsymbol{x}}_i)/2$; $\beta_0 = 2/3$ and $\beta_1 = 1/2$ if $\ddot{\boldsymbol{x}}(t)$ varies linearly from $\ddot{\boldsymbol{x}}_{i-1}$ to $\ddot{\boldsymbol{x}}_i$.

The following recursive equation for the time integration is reached introducing Eqs. (52) into Eq. (50).

$$\left[\beta_0\frac{\Delta t_i^2}{2}\boldsymbol{Z}_1 + \beta_1\Delta t_i\boldsymbol{Z}_2 + \boldsymbol{Z}_3\right]\Delta\ddot{\boldsymbol{x}}_i = -\boldsymbol{Z}_1\left[\boldsymbol{x}_{i-1} + \Delta t_i\dot{\boldsymbol{x}}_{i-1} + \frac{\Delta t_i^2}{2}\ddot{\boldsymbol{x}}_{i-1}\right] - \boldsymbol{Z}_2[\dot{\boldsymbol{x}}_{i-1} + \Delta t_i\ddot{\boldsymbol{x}}_{i-1}] - \boldsymbol{Z}_3\ddot{\boldsymbol{x}}_{i-1} + \boldsymbol{b}(p_i,t_i) + \overline{\boldsymbol{b}}(t_i) \tag{53}$$

Knowing the independent variables $\boldsymbol{x}_{i-1}$, their derivatives and the pore pressure at time t_{i-1}, an iterative process is necessary to evaluate them at time t_i:

- Vector $\boldsymbol{b}(p_i,t_i)$, cf. Eqs. (50), (45), (49), is approximated adopting the values of the pore pressure at time t_i obtained by the previous iteration; for the first iteration the value at time t_{i-1} is adopted to this purpose.
- Vector $\Delta\ddot{\boldsymbol{x}}_i$ is determined by solving Eq. (53), then $\boldsymbol{x}_i, \dot{\boldsymbol{x}}_i, \ddot{\boldsymbol{x}}_i$ are updated through Eqs. (52).
- The pore pressure rate $\dot{p}_i$ at the integration points of each element is evaluated through Eq. (46) and p_i is determined through Eqs. (52).
- Vector $\boldsymbol{b}(p_i,t_i)$ is updated and the next iteration is carried out.
- The process ends when vector $\boldsymbol{x}(t_i)$ and the pore pressure p_i stabilize.

Note that the pore pressure is not among the nodal variables of the finite element model. This, from the one hand, eliminates the consistency problems that could be encountered when both displacements and pore pressure are defined at the same element nodes. On the other hand, however, it requires the above mentioned iteration process.

With this respect it could be observed that, since the vast majority of geotechnical problems involves the elastic–plastic behavior of soil, an iterative process would be anyway necessary for the nonlinear analysis.

It seems necessary to observe that the described integration technique is less sophisticated than other approaches presented in the literature, see e.g. [23,24]. The fact that it performed satisfactorily is likely to depend on the small value of the time steps adopted for integrating the nonlinear problem and that a saving in overall computational time can be achieved by adopting the above mentioned methods.

8. Illustrative example

The two described finite element approaches have been applied to the test problem depicted in Fig. 1. It concerns one of the shallow excavations frequently used nowadays in Milan to host garages and other underground facilities. The excavation is carried into the granular subsoil adopting a cut-and-cover, top-down procedure, see e.g. [25,26]. Note that the lower part of excavation is well below the phreatic level.

The analysis is subdivided into two subsequent stages. First, the excavation process is simulated in static regime. Then, the effects of a seismic excitation are evaluated in the critical conditions in which the excavation has been completed but its bottom concrete slab has not been constructed yet.

The steps of excavation can be summarized as follows (cf. Fig. 1). First the reinforced concrete panels of the diaphragm walls (1) are set in place from the ground surface stabilizing the holes during excavation through bentonite slurry. Then a series of low pressure grouting injections (2) is performed from within the perimeter of the diaphragms. This forms a zone with reduced permeability necessary to limit the inlet of water when excavating below the water table. A few meter thick soil layer (3) is then

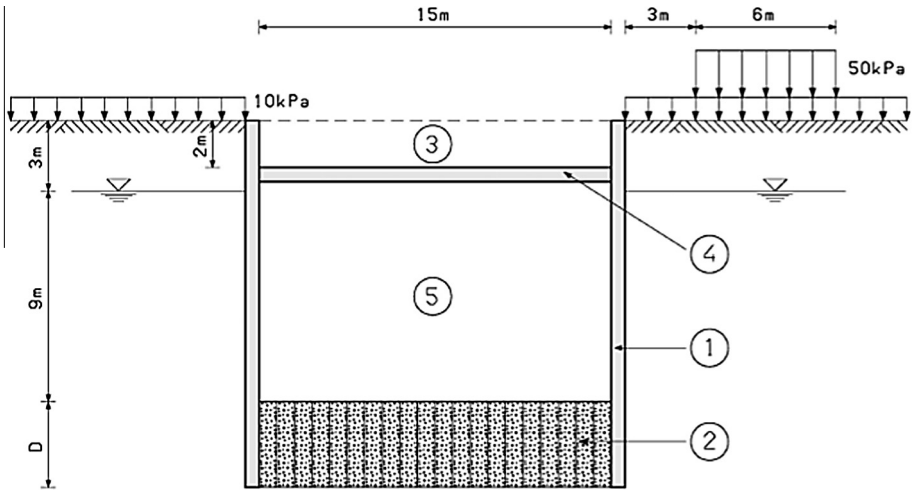

Fig. 1. Scheme of the shallow excavation supported by two diaphragm walls.

removed and the reinforced concrete top slab (4) is constructed and connected to the diaphragm walls. The soil (3) is set again in place to allow for the use of surface facilities (e.g. roads). The excavation is continued underneath the slab until reaching the layer of injected soil (2) on which the bottom concrete slab will be subsequently constructed.

The elastic–plastic analysis of this process was performed in plane strain regime and was based on a 105 m wide and 33 m deep rectangular mesh consisting of 1610 quadrilateral elements and 1704 nodes. Beam elements were used to model the concrete slab (4) and the 60 cm thick diaphragm walls (1).

The granular soil was divided into 6 horizontal layers, two of which are located above the water table. Each layer is assigned the mechanical properties evaluated at its mid depth according to the data provided by the Milan subway company for the design of underground facilities [27] or obtained by previous experimental studies [28]:

- Dry self weight of soil γ = 14.0 kN/m^3.
- Coefficient of earth pressure at rest $K_o = 0.5$.
- Elastic modulus of the natural soil E_s increasing with depth according to the following relationship where p_a is the atmospheric pressure and σ_{min} is the least value between vertical and horizontal effective stresses: $E_s = 2000 \cdot p_a \cdot \sqrt{\sigma_{\min}/p_a}$.
- Elastic modulus of the fully hardened grouted soil $E_g = 3E_s$.
- Negligible cohesion of the natural granular soil, which obeys Mohr–Coulomb yield condition.
- Effective friction angle of the natural soil $\phi_s = 35^\circ$.
- Cohesion of the grouted soil linearly increasing with depth according to the following relationship: c_g [kPa] $= 175. + 5.0 \cdot (\sigma_{\min}/p_a)$.
- Effective friction angle of the grouted soil $\phi_g = 33^\circ$.
- Coefficient of hydraulic conductivity of the natural soil $k_s = 5.0 \cdot 10^{-5}$ m/s.
- Coefficient of hydraulic conductivity of the grouted soil about two order of magnitude smaller than that of the natural soil.
- Non-associated flow rule for natural and grouted soils, with angle of plastic dilation equal to 10°.

After assigning to each soil element the geostatic effective stresses and pore pressure, the simulation of the excavation process initiates by "activating" the beam elements of the diaphragm walls (1) and by setting the properties of soil (2) to those of the injected soil. The possible volume change caused by the low pressure grouting was neglected.

The first excavation step concerns the soil of zone (3) above the water table. The "excavation forces" are determined by integrating the effective stresses and the self weight of the elements of this zone. The elements are subsequently removed from the mesh and the excavation forces are applied in small increments to the excavation contour.

The beam elements of the concrete slab (4) are then activated; the elements of soil (3) are set again in place, with their self weight, and the excavation of the upper layer of zone (5), below the slab but above the water table, is simulated.

Considering the relatively high permeability of the granular soil, no variation of the in situ pore pressure is accounted for during these elastic plastic analyses.

The excavation of the remaining layers of zone (5), located below the water table, requires a sequence of seepage and elastic plastic analyses.

First, a steady state seepage analysis evaluates the pore pressure distribution after the water table in the zone within the two diaphragm walls has been lowered to the bottom of the layer to be excavated. The water table level in the remaining part of the mesh is assumed to remain unchanged. In this analysis the diaphragm walls are seen as impervious zones.

For each excavation step the difference between initial and final pore pressure distributions is converted into nodal forces. These are added to the excavation forces determined by inte-grating the effective stresses and the self weight of the ele-ments to be excavated. These elements are subsequently removed from the mesh and a further elastic plastic analysis is performed by applying the previously calculated forces to the modified mesh.

At the end of the excavation process the base of the mesh was subjected to a horizontal sinusoidal acceleration with a frequency of 1 Hz and a peak value of 150 cm/s^2. The results of the dynamic analyses are summarized here in Figs. 2–5.

Figs. 2 and 3 show, respectively, the distributions of the horizontal effective pressure σ'_h acting on the diaphragm walls when the base acceleration reaches its maximum values in the leftward and in the rightward direction. In both cases the dynamic effective pressure is compared with the static one evaluated at the end of excavation. The diagrams of the dynamic water pore p on the diaphragm walls are reported in Figs. 4 and 5. Note that in these diagrams the effective stress and pore pressure have been divided by their maximum values, $\sigma'_{h,Max}$ and p_{Max}, attained at the end of excavation.

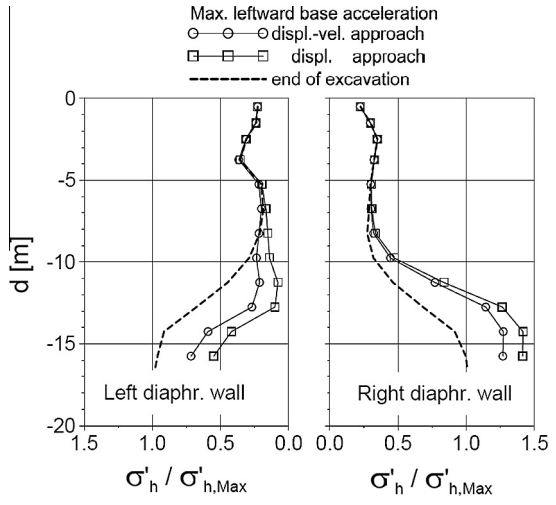

Fig. 2. Distributions of the horizontal effective pressure σ'_h on the diaphragm walls corresponding to the maximum base acceleration in the leftward direction ($\sigma'_{h,Max}$ is the maximum effective pressure at the end of excavation).

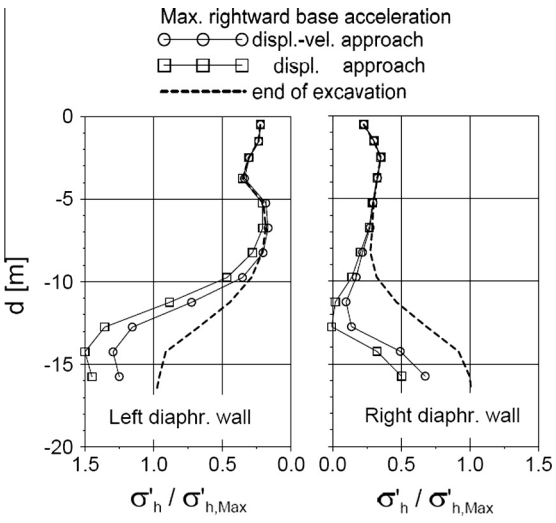

Fig. 3. Distributions of the horizontal effective pressure σ'_h on the diaphragm walls corresponding to the maximum base acceleration in the rightward direction ($\sigma'_{h,Max}$ is the maximum effective pressure at the end of excavation).

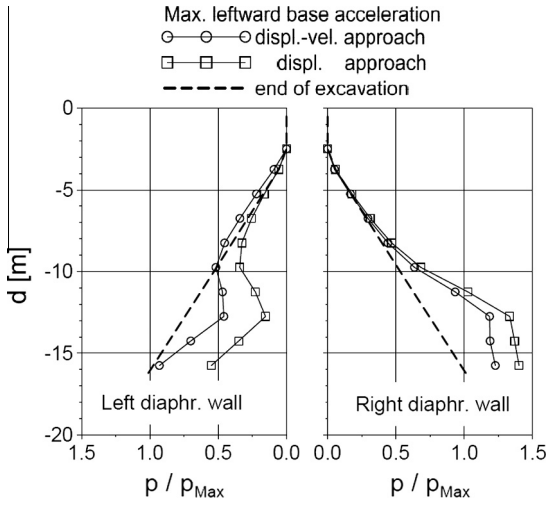

Fig. 4. Water pressure p distributions on the diaphragm walls corresponding to the maximum base acceleration in the leftward direction (p_{Max} is the maximum water pressure at the end of excavation).

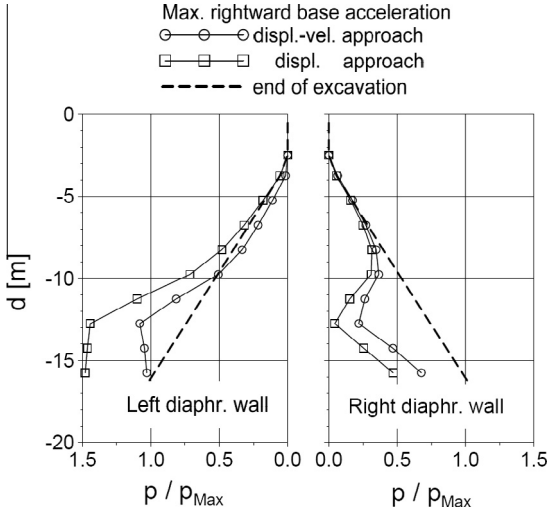

Fig. 5. Water pressure p distributions on the diaphragm walls corresponding to the maximum base acceleration in the rightward direction (p_{Max} is the maximum water pressure at the end of excavation).

The dynamic calculations show that the difference between the results of the two approaches increases with depth, reaching a maximum of about 15% for the effective stress and of 50% for the water pressure. Quite obviously, the results of the displacement-velocity formulation are the most accurate among the two. In fact, they do not depend on the additional simplifying assumptions which were introduced in the displacement approach.

Naturally, the accuracy of the displacement-velocity analysis has a cost. This depends on the fact that it involves a number of nodal variables which is twice than that of the displacement formulation. As a consequence, we have a non-negligible increase of the usage of core memory and of the required computation time (about 55% in the present case). This drawback, however, seems marginal considering the capacity of nowadays multi-processor and parallel computers and it would not represent a reasons for adopting the cheaper but less accurate algorithm.

9. Summary and conclusions

The finite element formulation of two-phase dynamic problems has been discussed on the basis of the assumption, customarily adopted in geotechnical engineering, that the saturated porous medium can be treated as the superposition of a liquid and of a solid phase.

After recalling the differential equations that govern the dynamic seepage flow of a liquid within a porous medium and the deformation of its skeleton, these equations have been coupled together and cast into a finite element form.

This led to a first approach that involves as nodal variables the displacements of the solid phase and the seepage velocity of the liquid phase. A second approach was then worked out, by neglecting some terms of the governing equations, in which the nodal variables are limited to the displacements of the solid phase only.

The two approaches, and a time integration scheme, have been presented in detail to allow the interested reader to follow the derivations and to implement them into his finite element codes.

The paper aimed also at comparing the computational burden and accuracy of the two mentioned approaches. To this purpose, a test problem was analyzed that concerns a shallow excavation supported by two diaphragm walls and carried out below the water table in a granular deposit.

Obviously, the displacement-velocity approach, which involves twice the independent variables of the displacement approach, turned out to be the most cumbersome one. In particular, for the dynamic analysis of the excavation problem it required a cpu time 55% larger than that necessary for the displacement approach.

On the other hand, the numerical results show a non-negligible difference. In fact, the maximum differences between the computed effective pressures on the diaphragm walls is around 15%, while the difference between the maximum pore pressures is close to 50%.

On the basis of these results, and considering that the displacement-velocity approach is the most accurate one among the two, it seems reasonable to conclude that it is not worth exploiting the computational saving permitted by the displacement formulation and that the more cumbersome displacement-velocity approach is preferable for the analysis of relevant dynamic problems involving saturated granular soils.

Appendix A. Application of Green–Gauss theorem

In order to derive Eqs. (36) and (41) consider a vectorial variable, say $\boldsymbol{u}$,

$$\boldsymbol{u}^T = \{\, u_x \quad u_y \quad u_z \,\} \tag{A.1}$$

and a tensorial variable, say $\boldsymbol{\sigma}$, which can be represented both in vector and matrix forms.

$$\boldsymbol{\sigma}_{vect}^T = \{\, \sigma_x \quad \sigma_y \quad \dots \quad \tau_{zx} \,\}; \quad \boldsymbol{\sigma}_{mat} = \begin{bmatrix} \sigma_{xx} & \tau_{xy} & \tau_{xz} \\ \tau_{yx} & \sigma_{yy} & \tau_{yz} \\ \tau_{zx} & \tau_{zy} & \sigma_{zz} \end{bmatrix} \tag{A.2,3}$$

The following relationship holds between the space derivatives (see List of Symbols) of the two above forms of $\boldsymbol{\sigma}$.

$$\boldsymbol{B}^T \boldsymbol{\sigma}_{vect} = (\nabla^T \boldsymbol{\sigma}_{mat})^T. \tag{A.4}$$

Consider now the space derivatives of the product of the two variables

$$\begin{aligned} \nabla^T (\boldsymbol{u}^T \boldsymbol{\sigma}_{mat})^T &= \boldsymbol{u}^T (\boldsymbol{B}^T \boldsymbol{\sigma}_{vect}) + (\boldsymbol{B}\boldsymbol{u})^T \boldsymbol{\sigma}_{vect} \\ &= \boldsymbol{u}^T (\nabla^T \boldsymbol{\sigma}_{mat})^T + (\boldsymbol{B}\boldsymbol{u})^T \boldsymbol{\sigma}_{vect} \end{aligned} \tag{A.5}$$

and integrate them over the volume Ω.

$$\int_\Omega \nabla^T (\boldsymbol{u}^T \boldsymbol{\sigma}_{mat})^T d\Omega = \int_\Omega \boldsymbol{u}^T (\boldsymbol{B}^T \boldsymbol{\sigma}_{vect}) d\Omega + \int_\Omega (\boldsymbol{B}\boldsymbol{u})^T \boldsymbol{\sigma}_{vect} d\Omega \tag{A.6}$$

Applying Green theorem to the left hand side integral of Eq. (A.6) one obtains.

$$\int_\Omega \nabla^T (\boldsymbol{u}^T \boldsymbol{\sigma}_{mat})^T d\Omega = \int_\Gamma \boldsymbol{u}^T \boldsymbol{T}_1 \boldsymbol{\sigma}_{vect} d\Gamma \tag{A.7}$$

Substitution of Eq. (A.7) into Eq. (A.6) leads to the following relationship, which is formally equivalent to those used in Eqs. (36) and (41)

$$\int_\Omega \boldsymbol{u}^T (\boldsymbol{B}^T \boldsymbol{\sigma}_{vect}) d\Omega = \int_{\Gamma_\sigma} \boldsymbol{u}^T \boldsymbol{T}_1 \boldsymbol{\sigma}_{vect} d\Gamma - \int_\Omega (\boldsymbol{B}\boldsymbol{u})^T \boldsymbol{\sigma}_{vect} \Omega. \tag{A.8}$$

List of symbols

Scalars

B_G	bulk modulus of grains
B_U	parameter governing the undrained volume change of the saturated porous medium
B_W	bulk modulus of water
k'	intrinsic permeability
k	hydraulic conductivity
n	volume (or effective) porosity
$n_{Ax},\ n_{Ay},\ n_{Az}$	surface porosities in the Cartesian directions
$n_u,\ n_w$	number of element nodes where displacements and discharge velocities are defined
p	pore pressure
$\overline{p}$	imposed boundary pore pressure on Γ_P
t	time
$\alpha_{xn},\ \alpha_{yn},\ \alpha_{zn}$	direction cosines of the outward vector normal to the surface Γ
$\alpha_{x'x}, \dots \alpha_{z'z}$	direction cosines of the local reference system axes $x',\ y',\ z'$ with respect to which boundary displacements and tractions are imposed
$\beta_0,\ \beta_1$	time integration coefficients
γ_W	unit weight of water
$\dot{\varepsilon}_{S,vol}$	volumetric strain rate of the solid phase
$\dot{\varepsilon}_{L,vol}$	volumetric strain rate of the liquid phase
μ_L	deviatoric viscosity of the liquid phase
μ_W	deviatoric viscosity of water
ρ_L	density of the liquid phase
ρ_G	density of grains
ρ_S	density of the solid phase
ρ_{Sat}	total density of the saturated porous medium
ρ_W	density of water
Ω	volume
Γ	surface
Γ_p	pervious boundary
Γ_u	displacement constrained boundary
Γ_w	impervious boundary
Γ_σ	loaded boundary

Differential operators

$$\boldsymbol{B} = \begin{bmatrix} \partial/\partial x & 0 & 0 \\ 0 & \partial/\partial y & 0 \\ 0 & 0 & \partial/\partial z \\ \partial/\partial y & \partial/\partial x & 0 \\ 0 & \partial/\partial z & \partial/\partial y \\ \partial/\partial z & 0 & \partial/\partial x \end{bmatrix}, \quad \nabla = \begin{Bmatrix} \partial/\partial x \\ \partial/\partial y \\ \partial/\partial z \end{Bmatrix}$$

Vectors (the superscript e denotes the eth finite element)

$\dot{\boldsymbol{e}}_L$	deviatoric strain rate of the liquid phase
$\boldsymbol{f}_D$	drag forces
$\boldsymbol{f}^e_{Lp},\ \boldsymbol{f}^e_{up}$	vectors depending on the pore pressure within the element
$\overline{\boldsymbol{f}}^e_{gSat}$	data vector depending on the weight of the saturated element
$\overline{\boldsymbol{f}}^e_{Lg}$	data vector depending on the weight of the liquid phase
$\overline{\boldsymbol{f}}^e_{Lp}$	data vector depending on the imposed boundary pore pressure
$\overline{\boldsymbol{f}}^e_t$	data vector depending on the imposed boundary tractions
$\overline{\boldsymbol{g}}$	acceleration of gravity
$\boldsymbol{m}^T =$	$\{1 \quad 1 \quad 1 \quad 0 \quad 0 \quad 0\}$
$\boldsymbol{u}$	displacements of the solid phase
$\overline{\boldsymbol{u}}$	imposed boundary displacements

(*continued on next page*)

$\bar{\boldsymbol{t}}$ imposed boundary tractions
$\boldsymbol{v}$ discharge velocity
$\boldsymbol{v}_W$ velocity of the water particles
$\boldsymbol{w}$ relative discharge velocity with respect to the skeleton
$\boldsymbol{w}_W$ relative velocity of the liquid particles with respect to the skeleton
$\dot{\boldsymbol{\varepsilon}}_S$ strain rate of the solid phase
$\dot{\boldsymbol{\varepsilon}}_L$ strain rate of the liquid phase
$\boldsymbol{\sigma}$ total stresses
$\boldsymbol{\sigma}'_S$ effective stresses
$\boldsymbol{\sigma}_L$ stresses of the liquid phase
$\boldsymbol{\tau}_L$ deviatoric stresses of the liquid phase

Matrices (the superscript e denotes the eth finite element)

$\boldsymbol{B}^e_w$, $\boldsymbol{B}^e_u$ derivatives of the interpolation functions of discharge velocity and displacements
$\boldsymbol{D}_S$ constitutive elastic matrix of the solid phase
$\boldsymbol{K}'$ intrinsic permeability matrix
$\boldsymbol{K}^e_S$ stiffness matrix of the solid element
$\boldsymbol{I}$ 6×6 identity matrix

$$\boldsymbol{I}_0 = \begin{bmatrix} 2 & 0 & 0 & 0 & 0 & 0 \\ 0 & 2 & 0 & 0 & 0 & 0 \\ 0 & 0 & 2 & 0 & 0 & 0 \\ 0 & 0 & 0 & 1 & 0 & 0 \\ 0 & 0 & 0 & 0 & 1 & 0 \\ 0 & 0 & 0 & 0 & 0 & 1 \end{bmatrix},$$

$$\boldsymbol{I}_1 = \begin{bmatrix} 4/3 & -2/3 & -2/3 & 0 & 0 & 0 \\ -2/3 & 4/3 & -2/3 & 0 & 0 & 0 \\ -2/3 & -2/3 & 4/3 & 0 & 0 & 0 \\ 0 & 0 & 0 & 1 & 0 & 0 \\ 0 & 0 & 0 & 0 & 1 & 0 \\ 0 & 0 & 0 & 0 & 0 & 1 \end{bmatrix}$$

$\boldsymbol{M}^e_{Sat}$ mass matrix of the saturated element
$\boldsymbol{M}^e_{Lwu}$, $\boldsymbol{M}^e_{Lww}$ element matrices depending on the density ρ_L of the liquid phase

$$\boldsymbol{N}_A = \begin{bmatrix} n_{Ax} & 0 & 0 \\ 0 & n_{Ay} & 0 \\ 0 & 0 & n_{Az} \end{bmatrix}$$

$\boldsymbol{S}^e_u$, $\boldsymbol{S}^e_w$ interpolation function matrices for displacement and discharge velocity components

$$\boldsymbol{T}_1 = \begin{bmatrix} \alpha_{xn} & 0 & 0 & \alpha_{yn} & 0 & \alpha_{zn} \\ 0 & \alpha_{yn} & 0 & \alpha_{xn} & \alpha_{zn} & 0 \\ 0 & 0 & \alpha_{zn} & 0 & \alpha_{yn} & \alpha_{xn} \end{bmatrix},$$

$$\boldsymbol{T}_2 = \begin{bmatrix} \alpha_{x'x} & \alpha_{x'y} & \alpha_{x'z} \\ \alpha_{y'x} & \alpha_{y'y} & \alpha_{y'z} \\ \alpha_{z'x} & \alpha_{z'z} & \alpha_{z'z} \end{bmatrix}, \boldsymbol{T}_2^{-1} = \boldsymbol{T}_2^T$$

$\boldsymbol{V}_S$ viscosity matrix of the solid phase
$\boldsymbol{V}_{SL}$ viscosity matrix of the coupled solid and liquid phases
$\boldsymbol{V}^e_{Sat}$ viscosity matrix of the saturated finite element
$\boldsymbol{V}^e_{Lwu}$, $\boldsymbol{V}^e_{Lww}$ element matrices depending on the deviatoric viscosity μ_L of the liquid phase

References

[1] Okabe S. General theory of earth pressures. J Jpn Soc Civil Eng 1926;12(1).
[2] Mononobe N, Matsuo H. On the determination of earth pressures during earthquakes. In: Proc world engineering congress, Tokyo, Japan, vol. 9; 1929. p. 176.
[3] Westergaard HM. Water pressures on dams during earthquake. Trans Am Soc Civil Eng 1933;98:418–34.
[4] Sandhu RS, Wilson EL. Finite element analysis of seepage in elastic media. J Eng Mech Div ASCE 1969;95(EM3):641–52.
[5] Desai CS. Finite element residual schemes for unconfined flow. Int J Numer Meth Eng 1976;10:1415–8.
[6] Zaman M, Gioda G, Booker J, editors. Modeling in geomechanics. Chichester, UK: John Wiley & Sons; 2000.
[7] Bear J. Dynamics of fluids in porous media. NewYork, USA: Dover Publications; 1988.
[8] Bird RB, Stewart WE, Lightfoot EN. Transport phenomena. New York, USA: John Wiley & Sons; 2007.
[9] Zienkiewicz OC, Bettess P. Soil and saturated media under transient, dynamic conditions; general formulation and the validity of various simplifying assumption. In: Pande GN, Zienkiewicz OC, editors. Soil mechanics – transient and cyclic loads: constitutive relations and numerical treatments. Wiley Series in Numerical Methods in Engineering; 1982.
[10] Zienkiewicz OC, Shiomi T. Dynamic behaviour of saturated porous media; the generalized Biot formulation and its numerical solution. Int J Numer Anal Meth Geomech 1984;8:71–96.
[11] Lewis RW, Schrefler BA. The finite element method in the static and dynamic deformation and consolidation of porous media. Chichester, UK: John Wiley & Sons; 1998.
[12] Zienkiewicz OC, Chan AHC, Pastor M, Schrefler BA, Shiomi T. Computational geomechanics with special reference to earthquake engineering. Chichester, UK: John Wiley & Sons; 1999.
[13] Stucchi R, Cividini A, Gioda G. Finite element approaches for the dynamic analysis of seepage. Ingegneria Sismica (Seism Eng) 2010;27(1):53–61.
[14] Cividini A, Gioda G. On the dynamic analysis of two-phase soils. In: Proc 3rd int symposium on computational geomechanics (ComGeo III), Krakow, Poland; 2013. p. 452–61.
[15] Cividini A, Gioda G. Seepage flow analysis in gravity and in variable acceleration fields. Ann Univ Bucharest (Math Ser), 2067-9009 2014;5(LXIII): 245–58.
[16] Nazem M, Carter JP, Airey DW, Chow SH. Dynamic analysis of a smooth penetrometer free-falling into uniform clay. Géotechnique 2012;62(10): 893–905.
[17] Sabetamal H, Nazem M, Carter JP, Sloan SW. Large deformation dynamic analysis of saturated porous media with applications to penetration problems. Comput Geotech 2014;55:117–31.
[18] Biot MA. General theory of three-dimensional consolidation. J Appl Phys 1941;12:155–64.
[19] Newmark NM. A method of computation for structural dynamics. J Eng Mech Div 1959;85(EM3):67–94.
[20] Wilson EL, Farhoomand I, Bathe KJ. Nonlinear dynamic analysis of complex structures. Earthquake Eng Struct Dyn 1973;1(3):241–52.
[21] Zienkiewicz OC, Wood WL, Taylor RL. An alternative single-step algorithm for dynamic problems. Earthquake Eng Struct Dyn 1980;8(1):31–40.
[22] Katona MG, Zienkiewicz OC. A unified set of single step algorithms – part 3: The beta-m method, a generalization of the Newmark scheme. Int J Numer Meth Eng 1985;21:1345–59.
[23] Chung J, Hulbert GM. A time integration algorithm for structural dynamics with improved numerical dissipation: the generalized-<alpha> method. J Appl Mech 1993;60:371–5.
[24] Kontoe S, Zdravkovic L, Potts DM. An assessment of time integration schemes for dynamic geotechnical problems. Comput. Geotech. 2008;35:253–64.
[25] Szechy K. The art of tunnelling. Budapest, Hungary: Akadémiai Kiadó; 1966.
[26] Vuchic VR. Urban transit systems and technology. New York, USA: John Wiley & Sons; 2007.
[27] Contini A, Cividini A, Gioda G. Numerical evaluation of the surface displacements due to soil grouting and to tunnel excavation. Int J Geomech ASCE 2007;7(3):217–26.
[28] Cividini A, Bonomi S, Vignati GC, Gioda G. Seepage-induced erosion in granular soils and consequent settlements. Int J Geomech ASCE 2009;9(4):187–94.